Electron Microscopy of a Family of Hexagonal Perovskites: One-Dimensional Structures Related to $Sr_4Ni_3O_9$

M. Huvé,* C. Renard,* F. Abraham,* G. Van Tendeloo,†,[1] and S. Amelinckx†

*Laboratoire de Cristallochimie et Physicochimie du Solide, ENSCL, Lille, BP 108, F-59652 Villeneuve d'Ascq Cedex, France. and
†EMAT, University of Antwerp (RUCA), Groenenborgerlaan 171, B-2020 Antwerp, Belgium

The structure of the compound $Sr_4Ni_3O_9$ can be described as a stacking of close-packed SrO_3 layers with omission of oxygens and insertion of nickel ions. The 4H structure can be considered as a translation interface modulated structure of a simpler basic structure. An incommensurate structure, based on the 4H structure, is attributed to a systematic "ledging" of the translation interfaces, similar to that causing the occurrence of incommensurability in long-period superstructures in alloys. This description also allows us to understand the transformation into the commensurate 4H structure after annealing. *In situ* heating inside the electron microscope transforms the 4H stacking into a disordered 9R- or 18R-type structure. Direct imaging by high-resolution electron microscopy confirms the structural models proposed for the different phases on the basis of their diffraction patterns.   © 1998 Academic Press

1. INTRODUCTION

Perovskite-related hexagonal phases can occur as different polytypes (1). Their symmetry is hexagonal (H) or rhombohedral (R), with lattice parameters showing simple relationships to those of the perovskite structure. The geometry of the stacking is based on simple geometric or crystallographic considerations and the common characteristic of these structures is that they all result from a linking of octahedra and trigonal prisms in various directions. The result is a wide variety of chemical systems in which we encounter several well known oxides such as $BaNiO_3$ (2H) (2), $BaRuO_3$ (9R) (3), $BaTiO_3$ (6H) (4), and $BaCrO_3$ (5H) (5). The indication within the first set of parentheses is stacking symbol.

For various reasons the (Ba, Sr)–(Ni, Ru)–O system is particularly interesting. The structures of this family of compounds are characterized by chains separated by strontium ions. The chains run along the c direction and consist of a succession of m octahedra and one face-sharing prism; they are linked together by (Sr, Ba)–O bonds. All members of

this series exhibit a hexagonal unit cell with an a parameter close to 9.5 Å. They differ from one another by the value of the c parameter, which corresponds to the stacking direction of the octahedra and prisms. All the members of the series can be described by the general formula $A_n(B_mC_l)O_x$, where n is the number of A ions between the chains per cell, m is the number of successive octahedra along the c direction, l is the number of successive prisms along the c direction, A denotes barium or strontium, B denotes ions in octahedral coordination, and C denotes ions in trigonal prismatic coordination. In no structure in this kind of compound has evidence been found of the occurrence of successive face-sharing prisms; therefore, the l value is taken to be 1.

The first member of the family was obtained for $m = 1$; an example is $Sr_3(Pt^{IV}Sr^{II})O_6$ ($a = 9.74$ Å, $c = 11.9$ Å) (6), where Pt^{IV} and Sr^{II} ions occupy respectively the octahedra and the prisms. Other compounds for $m = 1$ have also been isolated: $Ba_3(Pt^{IV}Ba^{II})O_6$ ($a = 9.314$ Å, $c = 11.204$ Å) (7); $Sr_3(Ir^{IV}Sr^{II})O_6$ ($a = 9.730$ Å, $c = 11.89$ Å) (8); etc. The number m of successive octahedra may be as large as 4 for $Ba_6(Ni_4Ni^{II})O_{15}$ ($a = 9.889$ Å, $c = 12.867$ Å) (9); the Ni oxidation state in the prisms is not well established. Up to now, no compound of $m > 4$ has been isolated. m is not always constant along the chains; therefore, the stacking sequence for $Sr_9Ni_{6.64}O_{21}$ can be described as a sequence of octahedra sharing opposite faces, $[Ni_3O_{12}]$ dimeric and $[Ni_2O_9]$ dimeric groups, which are connected through trigonal prisms (10).

The $m = 2$ members of this large family exhibit some structural peculiarities. The $Sr_4(Ru_2^V)O_9$ structure ($a = 9.889$ Å, $c = 12.867$ Å) (11) is made up of chains containing a succession of an empty prism and two octahedra. The compound $Sr_4(Ni_2^{III}(Na_{0.33}^INi_{0.33}^{III})O_{7.67}$ (12) is more complex; both sodium and nickel atoms occupy only two-thirds of the prismatic sites, and moreover, oxygen nonstoichiometry has been detected. In $Sr_4(Ni_2Ni_{0.5})O_9$ ($a = 9.474$ Å $c = 7.802$ Å) (13), 50% of the trigonal prisms are occupied by Ni ions, but the oxidation states of the nickel ions are not well established. For $Sr_4(Ni_2^{IV}Ni^{II})O_9$ ($a = 9.477$ Å and $c = 7.826$ Å) (14), all polyhedra are fully

[1] To whom correspondence should be addressed.

1

occupied. $Sr_5Ni_4O_{11}$ exhibits the same lattice parameters ($a = 9.480$ Å, $c = 7.815$ Å) (15), but no structure was determined as yet. It is probable that the structure is similar to that of the last two oxides. The last three oxides apparently are based on the same framework, the compositions being different however.

2. EXPERIMENTAL

The samples were prepared according to previously described method (15). Samples for electron microscopy were prepared by smoothly crushing in *n*-butanol the powder from which the $Sr_4Ni_3O_9$ single crystal was extracted. The TEM study was performed with a Jeol 200CX and high-resolution images were obtained using a Jeol 4000EX instrument, having a resolution of 1.7 Å. Simulated high-resolution electron microscopy (HREM) images were calculated using the Mac Tempas program.

3. STRUCTURAL CONSIDERATIONS

The mixed oxides of type Sr–Ni–O with composition around $Sr_4Ni_3O_9$ can be described in terms of close-packed layers with some omissions or substitutions. The geometry of such stackings has been discussed (1, 16). We briefly summarize these considerations in a form applicable to the present situation.

The structures can be considered as stackings of close-packed layers of composition SrO_3, each Sr ion being surrounded by six oxygens and each oxygen being surrounded by two Sr and four O neighbors (Fig. 1a). Such layers occur in many perovskite-like structures, the octahedral interstices being occupied by small cations such as Ti and Ni.

When describing these stackings we can focus attention on the Sr sites only. Successive layers of SrO_3 must be stacked in such a way that the separation of Sr ions is maximum; i.e., the Sr ions in one layer project along the normal in the center of a triangle of Sr ions in the adjacent layer. Ignoring the oxygen ions, i.e., considering only the sublattice of Sr ions, one can thus distinguish a cubic stacking $\Delta\Delta\Delta$ or $\nabla\nabla\nabla \cdots$ and a hexagonal stacking $\nabla\Delta$. In terms of the *ABC* stacking language these sequences are $ABC \cdots$ or $ABAB$ ($BCBC \ldots$ or $ACAC \ldots$). The former occurs in cubic perovskites, the latter in hexagonal perovskites. The stacking of the oxygen ions is of the same type as that of the Sr ions. A hexagonal stacking of SrO_3 layers considering Sr ions only is also hexagonally stacked when including also the oxygens. This follows from the fact that only one type of hollow, either Δ or ∇, can be filled by the full SrO_3 layer.

In the structures under consideration, trigonal prismatic configurations of oxygen atoms also occur along the same layers as the octahedral interstices. As pointed out (1), one can still formally use a description in terms of close-packed layers when introducing layers with omissions and substitu-

tions. A triangle of oxygen ions is hereby removed from the SrO_3 layer and replaced by a small cation such as nickel placed in the center of the "hole" created. If this is done according to a planar hexagonal lattice one obtains the result shown in Fig. 1b; such layers have the composition Sr_3NiO_6; they are designated by a dashed symbol such as A', B', and C'. Whereas undashed layers have hexagonal symmetry, the dashed layers have only threefold symmetry.

A sandwich $AB'A$ creates octahedral as well as trigonal prismatic interstices which can be filled by nickel, represented by a Greek letter. The trigonal prisms of oxygens are formed by the two undashed layers around the nickel ions contained in the dashed layer. Furthermore, two octahedral interstices in γ_o position are formed per unit mesh between the pairs of layers AB' and $B'A$. The full stacking symbol would thus read $A\gamma_o(B'\gamma_t)\gamma_o A$, where γ_o refers to an octahedral interstice and γ_t to nickel in a trigonal prismatic interstice. In a stacking consisting exclusively of A, A', ... , B, B' layers, the nickel atoms would thus form chains along c in γ_o positions ($B'\gamma_t$ means that in the B' layer the nickel atoms occupy γ positions). The stacking of parallel identical dashed layers, in which only the positions differ, such as $B'A'B'$, does *not* give rise to the formation of a lattice of triangular prismatic interstices; it is an unallowed stacking.

However, when forming a triplet of dashed layers including mirror images (indicated by the subscript m) forming a configuration such as $B'A'B'_m$, a hexagonal lattice of trigonal prismatic interstices, filled by nickel, is formed. Per unit mesh of this lattice there is between each pair of dashed layers one octahedral site. Furthermore, two lattices of "half"-trigonal prisms (in fact, trigonal pyramids), one above and one below the midplane of the sandwich, are formed within the same unit mesh at shifted positions 1/3 2/3 and 2/3 1/3. These "half"-trigonal prisms can be completed by superposing above and below an undashed layer leading to the configuration $|AB'A'B'_m|A \ldots$. At the same time two octahedral interstices per unit mesh are created between the dashed and undashed terminal layers, these can be occupied by nickel ions, and are located at positions 1/3 2/3 and 2/3 1/3.

The full stacking symbol $A\gamma_o(B'\gamma_t)\gamma_o(A'\gamma_t)\gamma_o(B'_m\gamma_t)\gamma_o \ldots$ describes in fact the structure of one of our phases (4H). Assuming full occupation of the available interstices its composition can be derived layer by layer as follows:

$$A = Sr_3O_9,$$
$$\gamma_o = 2Ni,$$
$$(B'\gamma_t) = Sr_3NiO_6,$$
$$\gamma_o = Ni,$$
$$(A'\gamma_t) = Sr_3NiO_6,$$
$$\gamma_o = Ni,$$
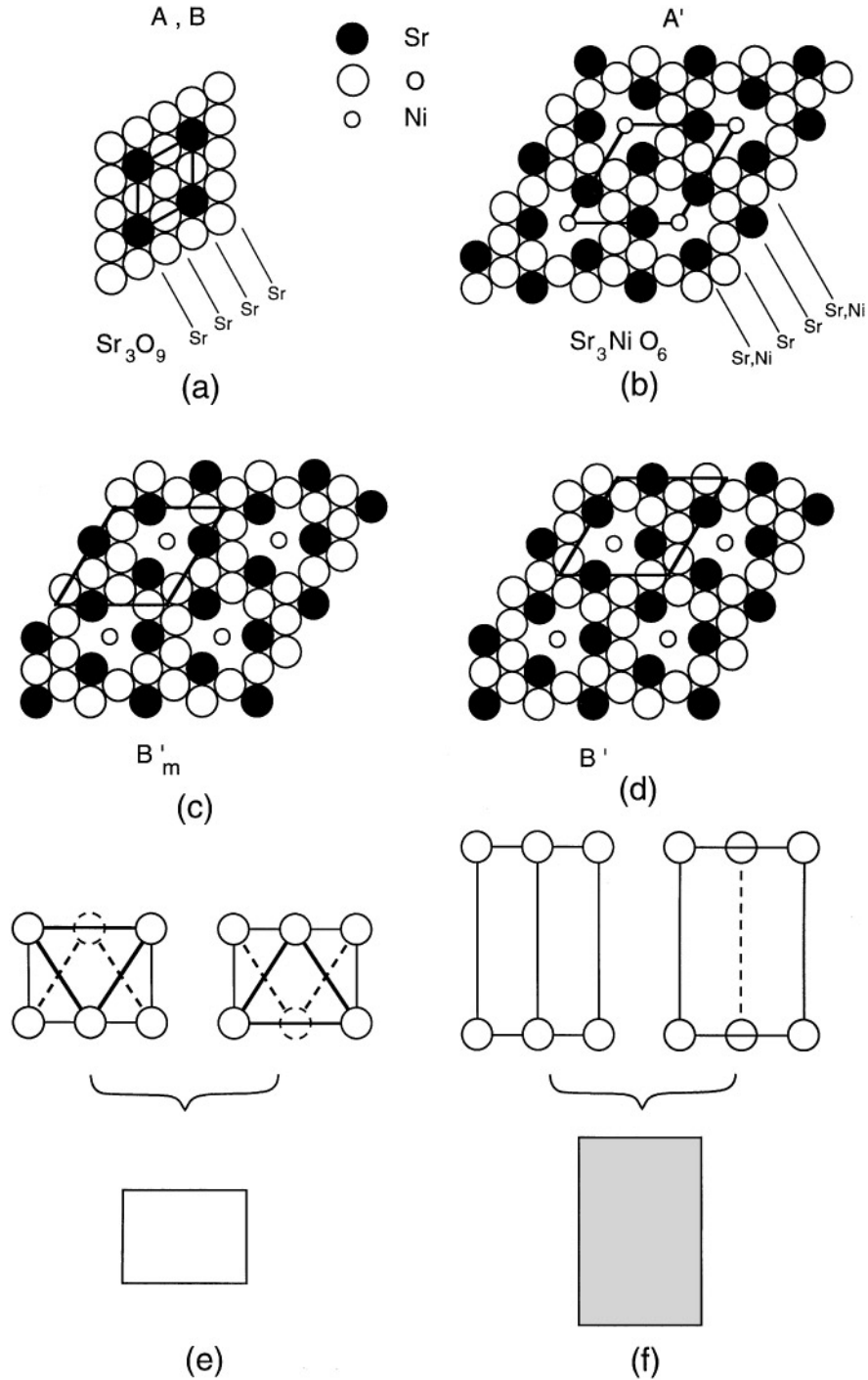$$(B'_m\gamma_t) = Sr_3NiO_6,$$
$$\gamma_o = 2Ni,$$
$$\text{i.e., } Sr_3Ni_4O_9.$$

FIG. 1. Schematic representation of the constituent layers the structure of $Sr_4Ni_3O_9$ and its derivatives. (a) A, B, ... , layers: A unit mesh with composition SrO_3 is outlined. (b) A', ... layer: A unit mesh with composition Sr_3NiO_6 is outlined. (c, d) B'_m and B' layers: The composition is the same as that of the A' layer and the unit mesh has been indicated; A' and B'_m are related by a mirror, B'_m and B' by a translation. (e) Simplified symbol representing the side view of octahedra. (f) Simplified representation of a side view of a trigonal prism.

It should be noted that all nickel ions are in the γ position; they form three chains parallel to c per unit mesh (see Fig. 2).

Charge neutrality requires that the average formal charge on nickel should be $10/3 = 3.33$. Since there are six nickel ions in octahedral sites and three in trigonal pyramidal sites, this average is achieved if the nickel in octahedral sites is assumed to be quadruply charged, and that in trigonal prismatic sites, charged two times.

If we assume the chains at the corners of the unit mesh $(0, 0)$ occupy γ positions, the other chains are at other γ positions in 1/3 2/3, 2/3 1/3 of the unit mesh; along each chain there are a succession of two face-sharing octahedra followed by a face-sharing trigonal prism. All chains, in the same positions with respect to the unit mesh, have their trigonal prism at the same level, but this level is different for chains at different positions, as represented schematically in Fig. 2a.

Transformation of a trigonal prismatic interstice into two octahedral ones is possible by the insertion of three oxygen-atoms in a "hole" of the dashed layer at the midplane of the trigonal prisms. This transforms locally a dashed layer into an undashed one, maintaining the layer stacking sequence. If a nickel ion is present in the interstice it can leave this interstice through a sideface and occupy a vacant octahedral site in a neighboring column. It is perhaps more probable that one of the two octahedral sites resulting from the oxygen insertion process may be occupied by nickel, leading to a redistribution of the linear arrangements of nickel ions in the "tunnels."

The sideways displacement of a prismatic interstice from one column to the adjacent one is thus possible by the local diffusion of three oxygen atoms out of an undashed layer, "punching" a hole in this layer (making it locally a dashed layer), to the neighboring trigonal prism, transforming the latter into two adjacent face-sharing octahedra. Simultaneously the vacancies created by the removal of the three oxygen atoms give rise to a "hole" and, thus, to a trigonal prism. Trigonal prismatic interstices can thus migrate by an oxygen vacancy diffusion mechanism, without changing the layer stacking mode.

The various structures, to be discussed below, are assumed to be closely related and to be all based on the hexagonal ($ABAB\ldots$) stacking of (O, Sr) layers of types $A(B)$ and $A'(B')$, as defined above. They can also be described in terms of a hexagonal packing of columns normal to these layers. Such columns consist of strings of isolated trigonal prisms of oxygen separated by a small number (i.e., 1, 2, 3, or 4) of face-sharing oxygen octahedra. In each of these phases all columns ideally have the same geometry; i.e., they all consist of the same succession of trigonal prisms and octahedra and all have the same length. In all phases the columns are arranged in a bundle according to similar hexagonal patterns; however, the geometry and the length of the columns are different in the different phases.

The columns are shifted along their length axes over either one or two structural units relative to the adjacent ones. As a result within the same layer trigonal prisms cannot occur in adjacent positions, i.e., cannot share edges in a projection such as Fig. 2a. This is implicit in the assumption that all models are based on the stacking of $A(B)$ and $A'(B')$ layers in the way described above. The proposed structural models are mostly rhombohedral and they can thus occur in two variants: obverse and reverse. This is consistent with the diffraction patterns along the
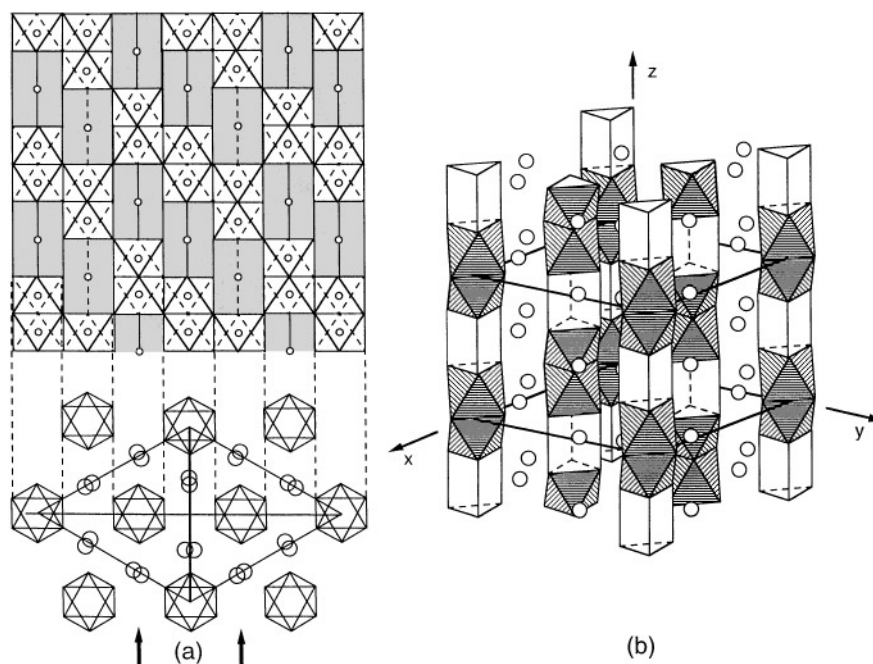

FIG. 2. Schematic representation of the 4H structure with ideal composition $Sr_4Ni_3O_9$. (a) Projections along the hexagonal axis and normal to it: the columns form a hexagonal array. Projection along a direction perpendicular to the c axis; the trigonal prisms are highlighted. (b) Spatial view: The columns of face-sharing oxygen octahedra and trigonal prisms are highlighted; they contain Ni atoms; Sr atoms occupy the spaces between these columns.

$[1\bar{2}10]$ zone (Figs. 3c, 3d), which only exhibit a center of symmetry. These empirical rules are suggested by the analysis of a number of known related structures, the so-called hexagonal perovskites (1), described in the Introduction.

We use extremely simplified schemes, representing only the projected positions of the trigonal prisms within the columns, it being understood that all lacking space along the columns is occupied by face-sharing oxygen octahedra. These schemes represent the projection along the $[10\bar{1}0]$ direction, indicated in Figs. 1a–1d, i.e., normal to the close-packed rows in the oxygen–strontium layers. The size of the unit mesh in the (00.1) plane implies that along such a direction only columns that are similarly positioned along the c direction superpose. From such a projection the spatial arrangement can be implied since the same projected structure must be obtained after a 120 rotation about the c axis, provided the structures have at least trigonal symmetry as assumed.

These structural principles are supported by the observation that the [00.1] pattern is similar in all phases (Fig. 3e) and by the fact that in all $[1\bar{2}10]$ zone patterns the same rectangle of prominently intense spots occurs (Fig. 3). The relation between our schemes and the [00.1] projection is illustrated in Fig. 2a.

Depending on the considered phase the projected unit mesh in direct space must thus contain $3 \times n$ ($n = 3, 4, 5$) elementary structural units. The projected oxygen octahedron is the elementary unit; a trigonal prism covers two such units.

4. INTERPRETATION METHOD FOR THE DIFFRACTION PATTERNS

In interpreting the diffraction patterns we repeatedly make use of the "fractional shift" method. In (17) it was shown that the diffraction pattern of an interface modulated structure consists of linear arrays of equidistant "satellite" reflections $\mathbf{h}$ associated with spots $\mathbf{g}$ of the "basic" structure. The diffraction vectors $\mathbf{h}$ of these "satellite" reflections are given by

$$\mathbf{h} = \frac{1}{\Delta}(m - \mathbf{g} \cdot \mathbf{R})\mathbf{e}_n, \qquad [1]$$

where $\mathbf{g}$ is a diffraction vector of the "basic" structure with which the satellite sequence is associated; Δ is the separation of the interfaces that are perpendicular to the unit vector $\mathbf{e}_n$; $\mathbf{R}$ is the displacement vector of the interfaces, assumed to be the same for all interfaces; and m is an integer characterizing the order of the satellite reflection.

According to kinematical theory (17) the intensity of the satellites decreases with increasing distance from the basic spot; i.e., the most intense spots are those for which $\mathbf{gR}$ (modulo 1), called "fractional shift" of the satellite sequence,

is the smallest. Due to dynamical beam interactions, intensity differences are attenuated, especially in "commensurate" patterns, but we see that nevertheless the latter rule is still obeyed in the examples discussed.

5. ELECTRON DIFFRACTION EVIDENCE

The [00.1] zone patterns have hexagonal symmetry (Fig. 3e); this geometry is the same for all phases. The spots of the first hexagon have significantly lower intensity than those of the second hexagon, which is consistent with the assumption that the structures are predominantly built on the stacking of ordered Sr_3O_9 close-packed layers. Also, the lattice parameter $a = 9.48$ Å is consistent with this assumption.

The $[1\bar{2}10]$ zone diffraction patterns of the different phases are reproduced in Fig. 3; this zone is the most useful one since it reveals the stacking of close-packed layers. We note that in all patterns the most prominent spots form a rectangle which has very nearly the same dimensions in all
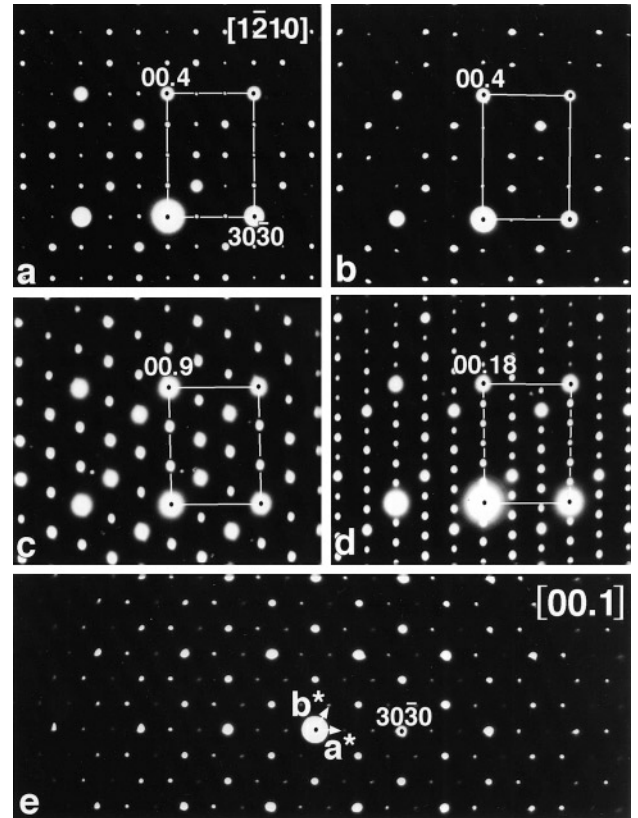

FIG. 3. Diffraction patterns of different phases with compositions in the vicinity of $Sr_4Ni_3O_9$. (a) Commensurate 4H. (b) Incommensurate 4H. (c) 9R. (d) 18R. Patterns a–d were made along the $[1\bar{2}10]$ zone. The same rectangle of intense spots is common to all patterns. (e) [00.1] zone pattern common to all phases. Note that the spots of the second hexagon are more intense than those of the first.
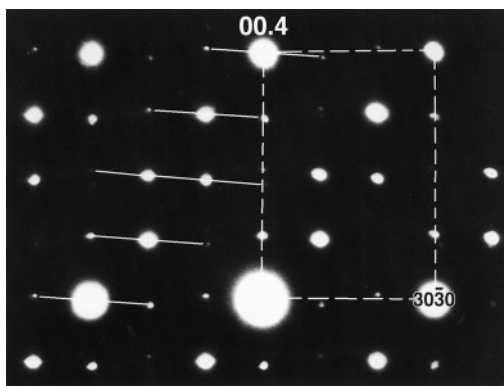
FIG. 4. Strongly incommensurate 4H diffraction pattern along $[1\bar{2}10]$ zone.

patterns. However, the ratio of length to width (L/W) is slightly different for the different phases, it is ~1.4 for Fig. 3a and 1.3 for Figs. 3c and 3d, suggesting a close relationship between the two latter structures.

The reciprocal mesh of this rectangle corresponds in direct space to the projected outline of an oxygen octahedron as represented schematically in Fig. 1e. The projected outline of a trigonal prism along the same zone is ideally twice as high as that of the octahedron, but its width is the

same (Figs. 1e, 1f). Below we often use the simplified representations introduced in Fig. 1. The presence of this common rectangle of prominently intense spots suggests that the different phases are built on a common motive, the oxygen octahedron and the trigonal prism, which is dimensionally closely related to the octahedron.

In all patterns the width of the rectangle is divided in three intervals by spot rows. The length of the rectangle may contain either 3 (Fig. 3c), 4 (Fig. 3a), or 6 (Fig. 3d) intervals, suggesting different stacking periods. Figure 3a is typical of a hexagonal lattice; we call the corresponding phase 4H. Figures 3c and 3d are typical of rhombohedral lattices; we call the corresponding phases respectively 9R and 18R.

The pattern of Fig. 4 looks commensurate, as do the patterns of Figs. 3a, 3c, and 3d; however, the pattern of Fig. 3b or 4, which is very similar to the pattern of Fig. 3a, is slightly incommensurate. As a result of the incommensurability, dynamical interactions between diffracted electron beams, which tend to equalize the intensities of spots, are suppressed; consequently the intensity differences between spots are much more pronounced in Figs. 3b and 4, compared with the commensurate pattern of Fig. 3a. The incommensurability is an important feature because it indicates that this structure can be derived by modulation from a simpler structure; as will be shown below. Moreover,
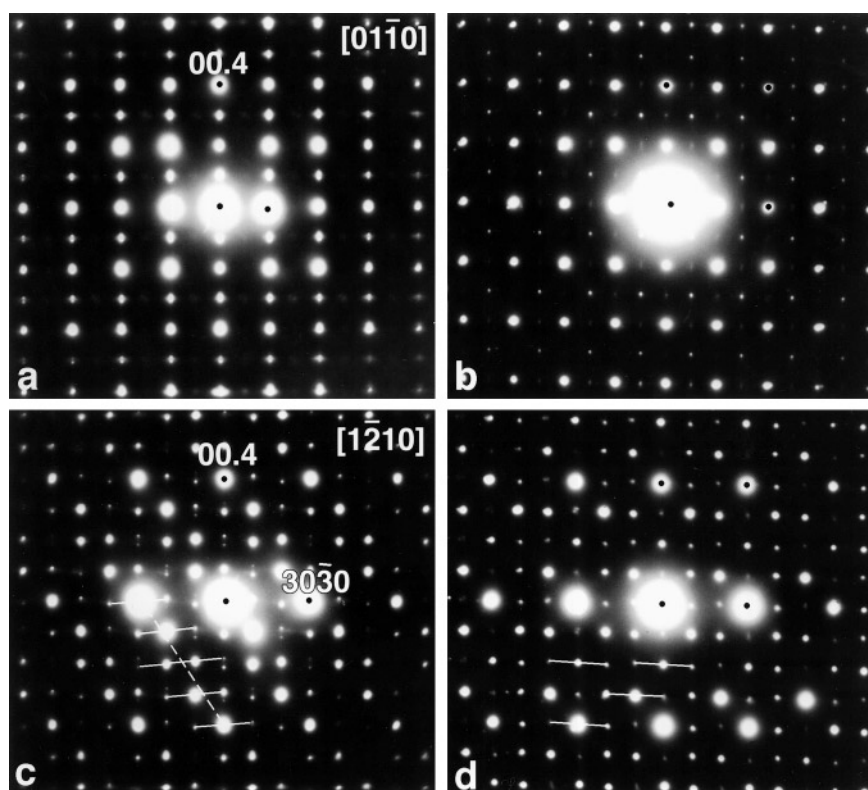

FIG. 5. Diffraction patterns of phases 4H (a, c) and 4M (b, d) along two different zones, $[10\bar{1}0]$ and $[1\bar{2}10]$. The patterns refer to the same specimen area before (4H) and after (4M) heat treatment above 400°C. Note that the slope of the satellite sequences is different in (c) and (d).
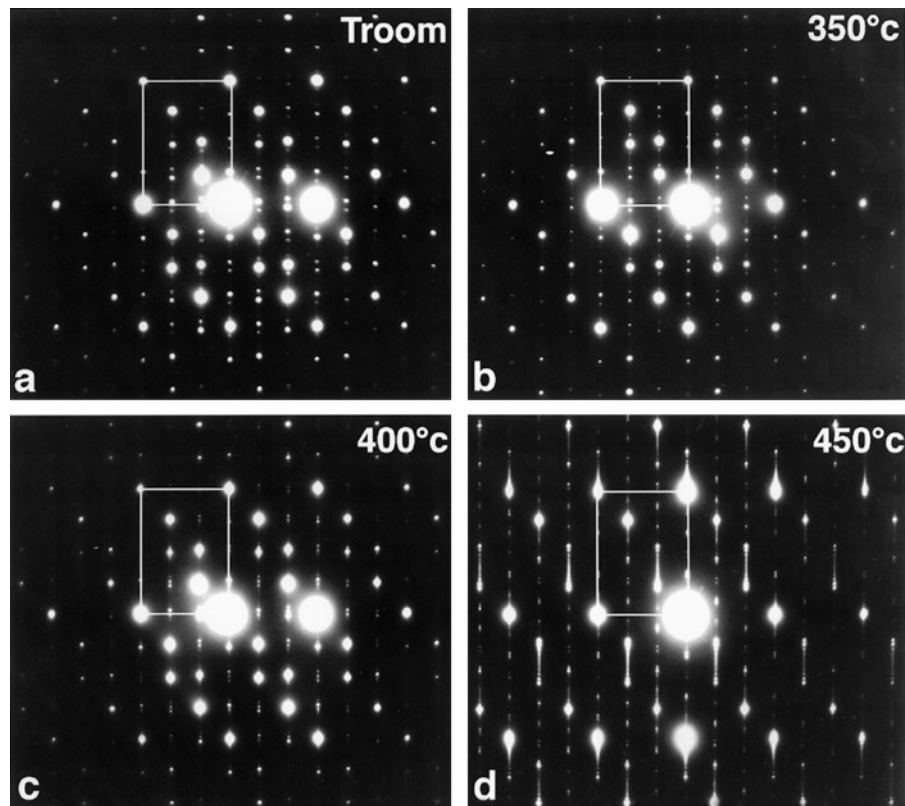
FIG. 6. Evolution of the $[1\bar{2}10]$ zone diffraction pattern of 4H on heating. (a) Room temperature; the pattern is incommensurate. (b) 350°C. (c) 400°C. (d) 450°C. Note the presence of a common rectangle of intense spots.

it allows us to deduce the spot positions of this hypothetical simpler structure.

Another remarkable feature common to all patterns is the relatively larger intensity of the spots situated close to one diagonal of the rectangle of prominent spots. The common parent phase must therefore have intense spots along this diagonal. This is also supported by the observation that the diffraction spots can be considered as equispaced sequences, associated with positions along this diagonal (Fig. 4).

Heating the sample produces the 4M pattern of Fig. 5d. A heating sequence is reproduced in Fig. 6. The initial pattern is rather strongly incommensurate (Fig. 6a). As the temperature increases, sequences of closely spaced spots are formed around the original spot positions. Finally at 450°C streaks are formed along the c^* direction, suggesting disorder in the layer sequences. Furher heating establishes a different phase where all diffuse scattering has disappeared (Fig. 5d), but which is apparently closely related to the initial 4H phase. However, in fact, a different phase has resulted. On close inspection Fig. 5d is no longer due to a hexagonal lattice since the spot rows are no longer mutually perpendicular. Moreover, a slight noncommensurability remains. The corresponding phase is presumably monoclinic. On cooling this phase is maintained.

When comparing the $[01\bar{1}0]$ zone patterns before (Fig. 5a) and after (Fig. 5b) heat treatment, it becomes evident that a different phase has been formed. The similarity of the lattice parameters and of the intensity distribution in the spots suggests that this monoclinic structure differs only in small details from the 4H structure and is presumably a differently ordered derivative of it.

6. ANALYSIS OF THE DIFFRACTION PATTERNS

The 4H Pattern (Fig. 3a)

The lattice parameters deduced from this diffraction pattern ($a = 9.48$ Å, $c = 7.83$ Å) are consistent with those of the structure described in (15) and attributed to the compound with a composition close to Sr$_4$Ni$_3$O$_9$. This compound is isostructural with Sr$_4$Ru$_2$O$_9$ (11) and Sr$_4$Ni$_{2.5}$O$_9$ (13), the composition differences being attributed to the presence of vacancies in the Ni(Ru) sublattice. Using the simplified structure schemes introduced above (Fig. 1) the projected structure can be represented as in Fig. 7. The corresponding stacking symbol can be written as $A\gamma_o(B'\gamma_t)\gamma_o(A'\gamma_t)\gamma_o(B'_m\gamma_t)\gamma_o$, or in short notation, $AB'A'B'$

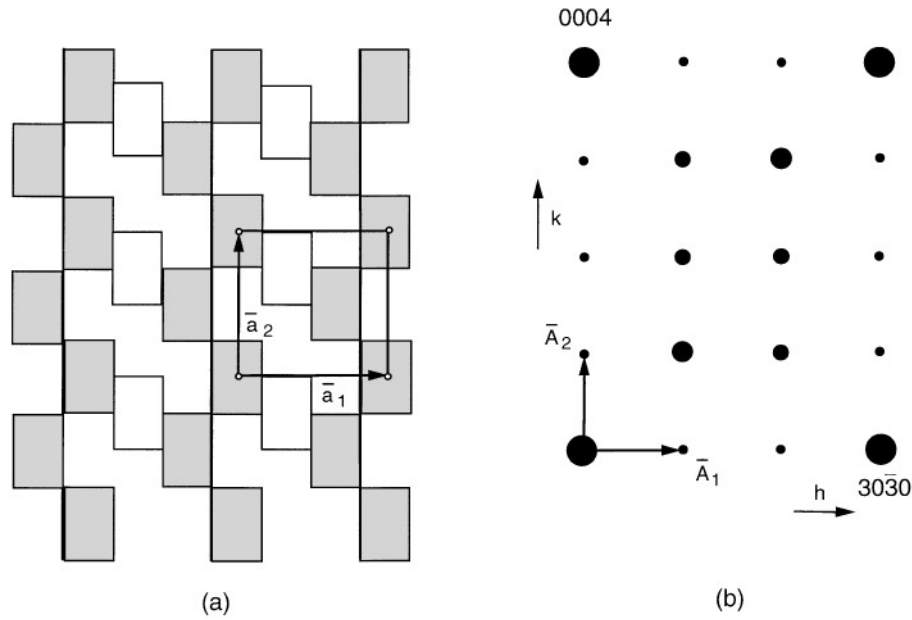We now show that the 4H structure can be regarded as a commensurate interface modulated structure obtained

FIG. 7. Structure of the 4H phase. (a) Schematic model with unit mesh $(\mathbf{a}_1, \mathbf{a}_2)$. (b) Diffraction pattern: The size of the dots is proportional to the relative intensities of the spots. The unit mesh is $(\mathbf{A}_1, \mathbf{A}_2)$.

from a related hypothetical simpler structure of the same family, by the periodic introduction of conservative planar translation interfaces. We hereby make use of the theoretical considerations developed in Section 4. This is not merely an academic exercise since it allows us to understand the occurrence of slightly incommensurate diffraction patterns in most 4H samples and also allows us to explain why annealing in vacuo may lead to a commensurate pattern.
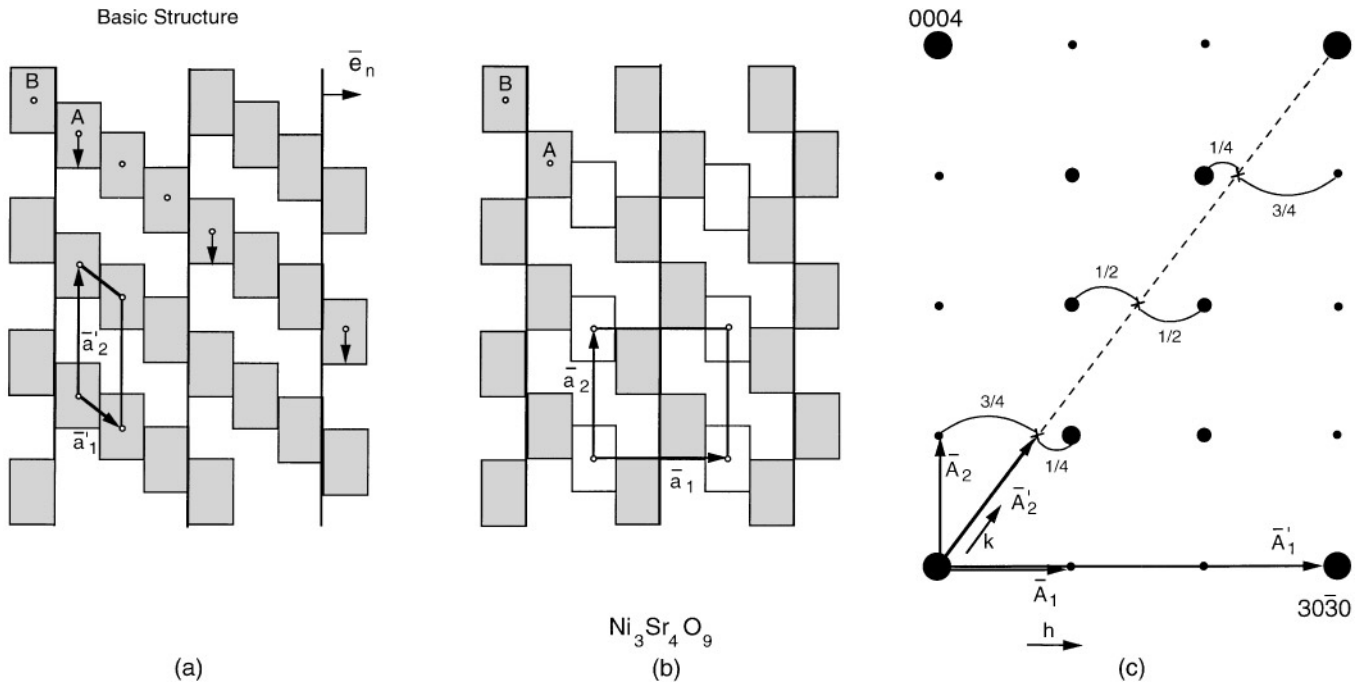

FIG. 8. Projected 4H structure as derived from a simple basic structure. (a) Basic structure with unit mesh $(\mathbf{a}_1', \mathbf{a}')$. The conservative planar interfaces are represented by heavy lines. The associated displacements are represented by vectors. (b) The projected 4H structure resulting from the crystallographic shear process represented in (a). The unit mesh $(\mathbf{a}_1, \mathbf{a}_2)$ is indicated. (c) Schematic representation of the diffraction pattern of 4H. The positions of the spots due to the "basic" structure are indicated by crosses; the unit mesh is $(\mathbf{A}_1', \mathbf{A}_2')$. The base vectors of the reciprocal lattice of 4H are $(\mathbf{A}_1, \mathbf{A}_2)$. The fractional shifts are indicated.

The symplest hypothetical "basic" structure consists of a periodic arrangement of columns consisting of two face-sharing octahedra followed by one face-sharing trigonal prism. The primitive unit mesh $(\mathbf{a}'_1, \mathbf{a}'_2)$ of the projection is indicated in Fig. 8a. The reciprocal unit mesh $(\mathbf{A}'_1, \mathbf{A}'_2)$ is given in Fig. 8c. It is clear that spots occur only along one diagonal of the basic rectangle. The ideal composition of this structure is $Sr_4Ni_3O_9$. The sense of inclination of this spot sequence is consistent with the intensity distribution of Fig. 4. These sequences of spots are obviously perpendicular to the planes of high scattering power in the structure.

We now introduce in the structure of Fig. 8a conservative translation interfaces parallel to the c direction, with a displacement vector of $\pm 1/4\, c$, as represented schematically in Fig. 8a. According to expression [1] linear satellite sequences perpendicular to these interfaces are now associated with each of the basic spots. The spacing in the spot sequence is then $1/\Delta = 4/3a, \ldots$, the fractional shifts associated with the diffraction vector $\mathbf{g}$ being given by $\mathbf{g} \cdot \mathbf{R} = k/4$. This leads to the values $\mathbf{g} \cdot \mathbf{R} = \frac{1}{2}, \frac{2}{4}, \frac{3}{4}$, respectively for the successive rows of spots $k = 1$, $k = 2$, $k = 3$ perpendicular to c. This result is trivial; it reproduces the commensurate diffraction pattern of 4H. Also, the relative spot intensities, as predicted by the considerations of Section 4, are well reproduced; the most intense spots are those with the smallest fractional shift, $\mathbf{g} \cdot \mathbf{R} = \pm 1/4$, followed by those with $\mathbf{g} \cdot \mathbf{R} = \pm 1/2$; they are located close to the diagonal of the rectangle as represented schematically in Fig. 8c by the size of the dots and observed in Figs. 3a and 4.

We note that in the observed incommensurate diffraction patterns (Fig. 4) the spot rows parallel to c^* are affected very little, whereas the spot rows roughly perpendicular to c^* are in fact inclined over a small angle with respect to that direction. Following the logic of the model the satellite rows are perpendicular to the prismatic interfaces, with the fractional shifts mentioned above, but which are now slightly inclined with respect to the c direction; the layer planes maintain their direction. This change in orientation of the prismatic planes is brought about by systematic "ledging" of these planes as represented schematically in Fig. 9, where the trigonal prisms have been highlighted to make the figure more readable. The angle of inclination of the satellite rows will depend on the average separation of ledges, i.e., separation of the layers at which such a lateral shift occurs. This angle is therefore variable. A change in orientation of the interfaces is accompanied by a slight decrease in average separation of these interfaces and therefore the intersatellite separation is somewhat larger than in commensurate 4H. As a result, not only an "orientation anomaly" but also a small "spacing anomaly" occurs. Both can be observed in Fig. 4 where the inclination angle is particularly large.
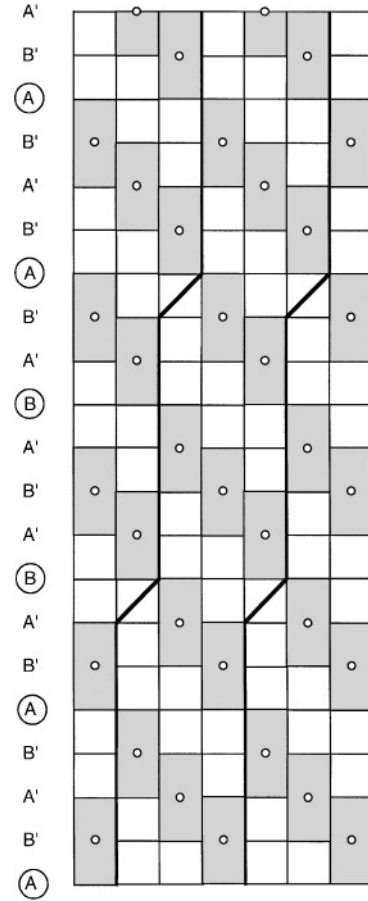

FIG. 9. Systematic "ledging" of the planar interfaces occurring in the incommensurate 4H structure, when interpreted as a shear structure.

With the change in orientation is associated a change in local stoichiometry, since at the level where the lateral shift of the interface occurs, a cluster of three face-sharing octahedral interstices can be formed instead of the cluster of two in the commensurate structure. The columns of face-sharing polyhedra then contain periodically a cluster of three octahedra instead of two in the commensurate structure. Depending on the sense of the ledges, either clusters of three successive octahedra or single octahedra are formed (Fig. 10). The changes in stoichiometry accompanying the ledge formation are thus opposite in these two cases.

The 9R Structure

The primitive unit mesh $(\mathbf{A}_1, \mathbf{A}_2)$ of the diffraction pattern is shown in Fig. 11c with respect to the basic rectangle of prominent spots. The unit mesh in direct space $(\mathbf{a}_1, \mathbf{a}_2)$ derived from this diffraction pattern is represented in Fig. 11b with respect to the basic building unit, which is the projected octahedron.
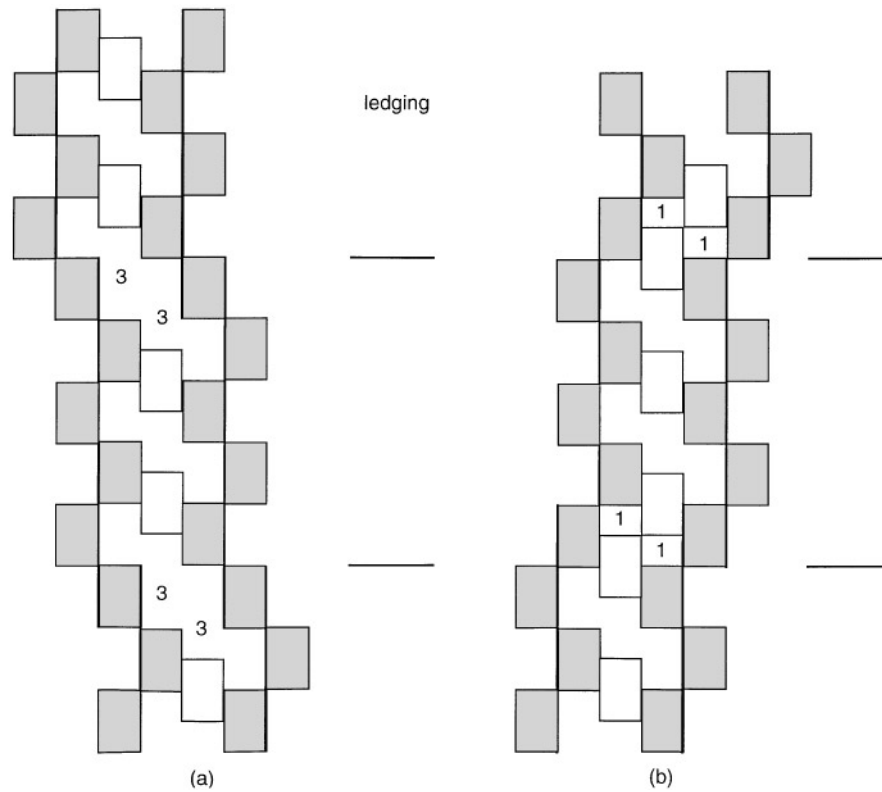
FIG. 10. Depending on the sense of inclination of the interfaces, ledging can lead to deficiency (a) or to excess (b).
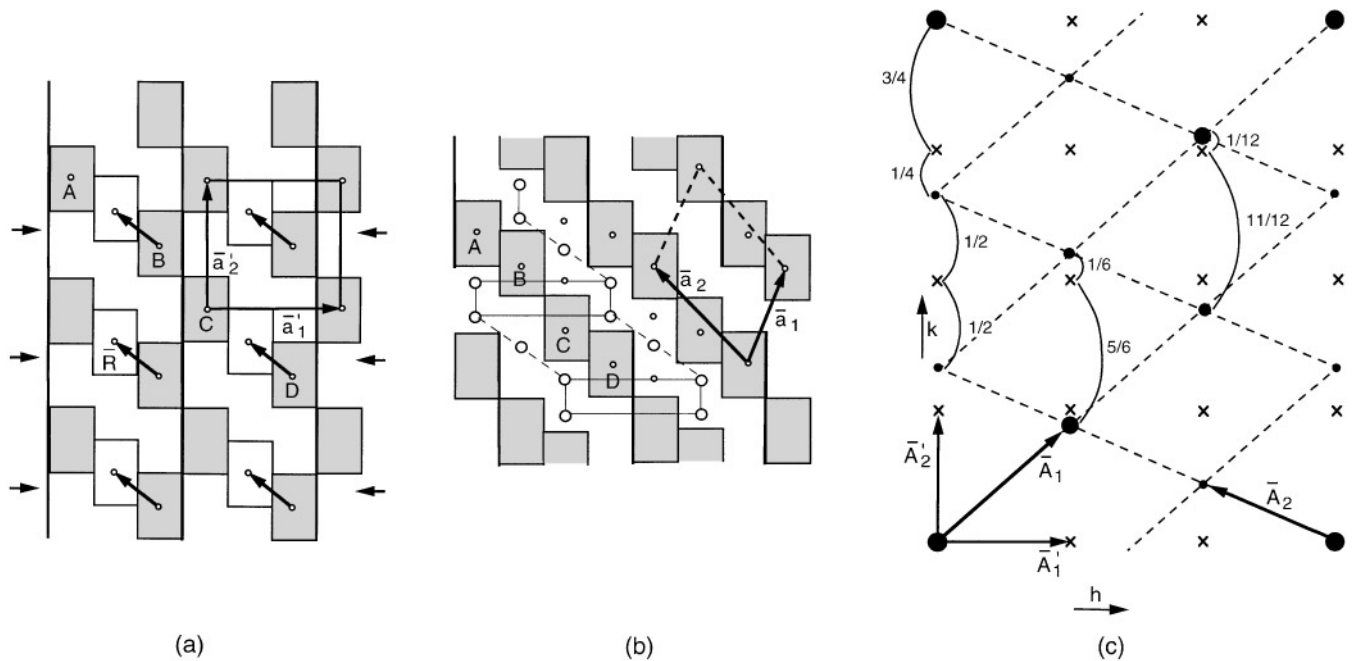

FIG. 11. Projection of the 9R structure as a derivative of the 4H structure. (a) Schematic representation of the basic 4H structure: The 4H unit mesh $(\mathbf{a}'_1, \mathbf{a}'_2)$ is outlined. The levels of the nonconservative interfaces are indicated by arrows; the associated displacement vectors $\mathbf{R}$ are indicated as well. (b) Projection of the 9R structure obtained as a result of the crystallographic shear process represented in (a). The unit mesh $(\mathbf{a}_1, \mathbf{a}_2)$ of the projected structure is outlined. (c) Schematic representation of the diffraction pattern of 9R. The positions of the 4H spots are shown by crosses. The fractional shifts of the 9R spots are indicated. The base vectors $(\mathbf{A}'_1, \mathbf{A}'_2)$ of the reciprocal lattice of the 4H structure and the base vectors $(\mathbf{A}_1, \mathbf{A}_2)$ of the reciprocal lattice of the 9R structure are represented.

Applying the empirical stacking rules and taking in particular into account the restrictions on the relative positions of trigonal prisms, it is possible to propose the projected structure shown in Fig. 11b. When comparing this model with the model resulting from Fig. 11a by the introduction every third layer of (0001) interfaces with the indicated displacement vector $(\mathbf{R} = -\frac{1}{3}\mathbf{a}'_1 + \frac{1}{4}\mathbf{a}'_2)$ it becomes clear that the 9R structure can be described as a commensurate interface modulated superstructure of the 4H structure. To check this assumption the diffraction pattern derived from this model was compared with the observed one.

According to the theoretical considerations of Section 4 the diffraction pattern of this interface modulated structure should consist of linear sequences of spots along c^* with a spacing of one-third of the length of the basic rectangle of spots and they should be fractionally shifted over $\mathbf{g}\cdot\mathbf{R} = -\frac{1}{3}h + \frac{1}{4}k$. It is clear from Figs. 11c and 3c that this is indeed the case and that moreover the spot intensities decrease with increasing $\mathbf{g}\cdot\mathbf{R}$, as required by the theory. This strongly suggests that the model is correct. If the three-dimensional structure is taken into account then the actual sequence is evidently 18R. The stacking sequence of the corresponding spatial model can be formulated as $AB'A'$ $BA'B'A$. The corresponding composition is $Sr_9Ni_7O_{21}$. The unit cell c parameter is about 35.1 Å.

The 18R Structure

The primitive unit mesh $(\mathbf{A}_1, \mathbf{A}_2)$ of the diffraction pattern is shown in Fig. 12c with respect to the basic rectangle of prominent spots. The unit mesh in direct space $(\mathbf{a}_1, \mathbf{a}_2)$ deduced from this pattern is indicated in Fig. 12b with respect to the basic building unit mesh, which is the projected octahedron. Using the empirical stacking rules discussed in Section 3, a projected structure can be proposed (Fig. 12b). This model results from the structure of 4H by introducing every sixth layer an interface on (00.1) with the indicated displacement vector $(\mathbf{R} = \frac{1}{3}\mathbf{a}'_1 + \frac{1}{2}\mathbf{a}'_2)$ (Fig. 12a). The 18R structure can thus be considered as a commensurate interface modulated derivative of the 4H structure. The theoretical composition is the same as that of the 9R structure, i.e., $Sr_9Ni_7O_{21}$; however, the geometry of the strings of polyhedra is different; in the 9R structure we have along each column the succession P–O–O–P–O–O–O–..., whereas in 18R this succession is P–O–O–P–O–O–P– O–O–O–P–O–O–O– ... . The c parameter is also 35.1 Å. One type of column can be transformed into the other one by the conversion of one pair P–O into O–P.

The theoretical pattern, as deduced by the fractional shift method, is shown in Fig. 12c. The fractional shift is in this case given by $\mathbf{g}\cdot\mathbf{R} = \frac{1}{3}h + \frac{1}{2}k$. Note also that the relative
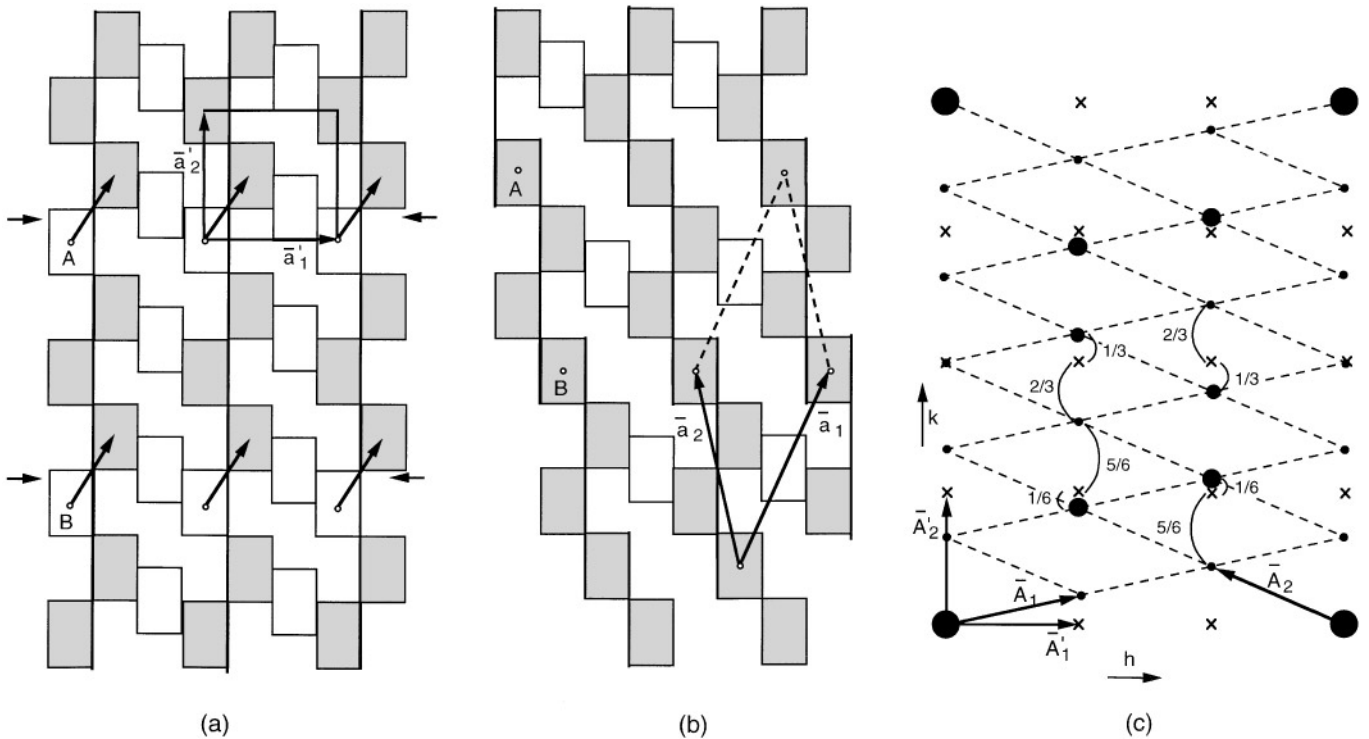

FIG. 12. Projection of the 18R structure obtained as a derivative of the 4H structure. (a) Basic 4H structure: The unit mesh $(\mathbf{a}'_1, \mathbf{a}'_2)$ is outlined. (b) Projection of the 18R structure as derived by the shear process outlined in (a). The unit mesh $(\mathbf{a}_1, \mathbf{a}_2)$ is indicated. (c) Schematic representation of the diffraction pattern of 18R. The positions of the spots due to the basic 4H structure are indicated by crosses; its unit mesh is $(\mathbf{A}'_1, \mathbf{A}'_2)$. The unit mesh of the 18R diffraction pattern is $(\mathbf{A}_1, \mathbf{A}_2)$. The fractional shifts are indicated.
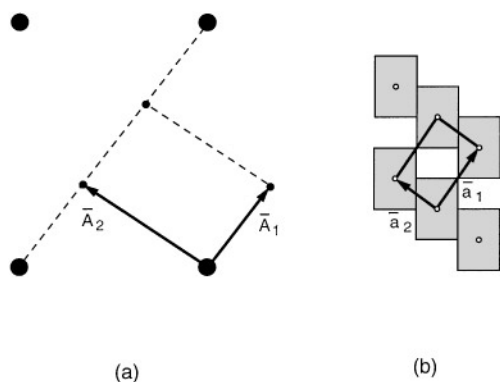
FIG. 13. Projection of the 3R structure. (a) Diffraction pattern. The unit mesh is $(\mathbf{A}_1, \mathbf{A}_2)$. (b) Structural model deduced from (a); the unit mesh is $(\mathbf{a}_1, \mathbf{a}_2)$.

intensities in Fig. 3d agree with those predicted by the model. The unit cell c parameter is about 11.7 Å.

The 3R Structure

In specimens that have been beam heated in the microscope, usually phase separation takes place; bands that are limited by (00.1) planes are formed and exhibit a different structure. This can readily be concluded from high-resolution images, to be discussed below. The bands are too narrow to allow the production of a separate electron diffraction pattern, but the Fourier transform of the high-resolution image shows that the diffraction pattern exhibits again the same rectangle of intense spots, as well as two more spots dividing one of the diagonals of the rectangle into three intervals. This pattern is represented schematically in Fig. 13a. The unit mesh in direct space $(\mathbf{a}_1, \mathbf{a}_2)$ deduced from this pattern and the corresponding structure are represented in Fig. 13b. The columns now consist of the alternation of trigonal prisms and octahedra in the proportion $1:1$. The theoretical composition, assuming all interstices to be filled, is $Sr_3Ni_2O_6$; its stacking symbol is $A'B'$.

The 4M Structure

The diffraction pattern of Fig. 5d is obtained at room temperature after a heating cycle to 450°C, starting from an incommensurate 4H sample; it is apparently closely related to that of the 4H structure (Fig. 4 or 5c) as far as the
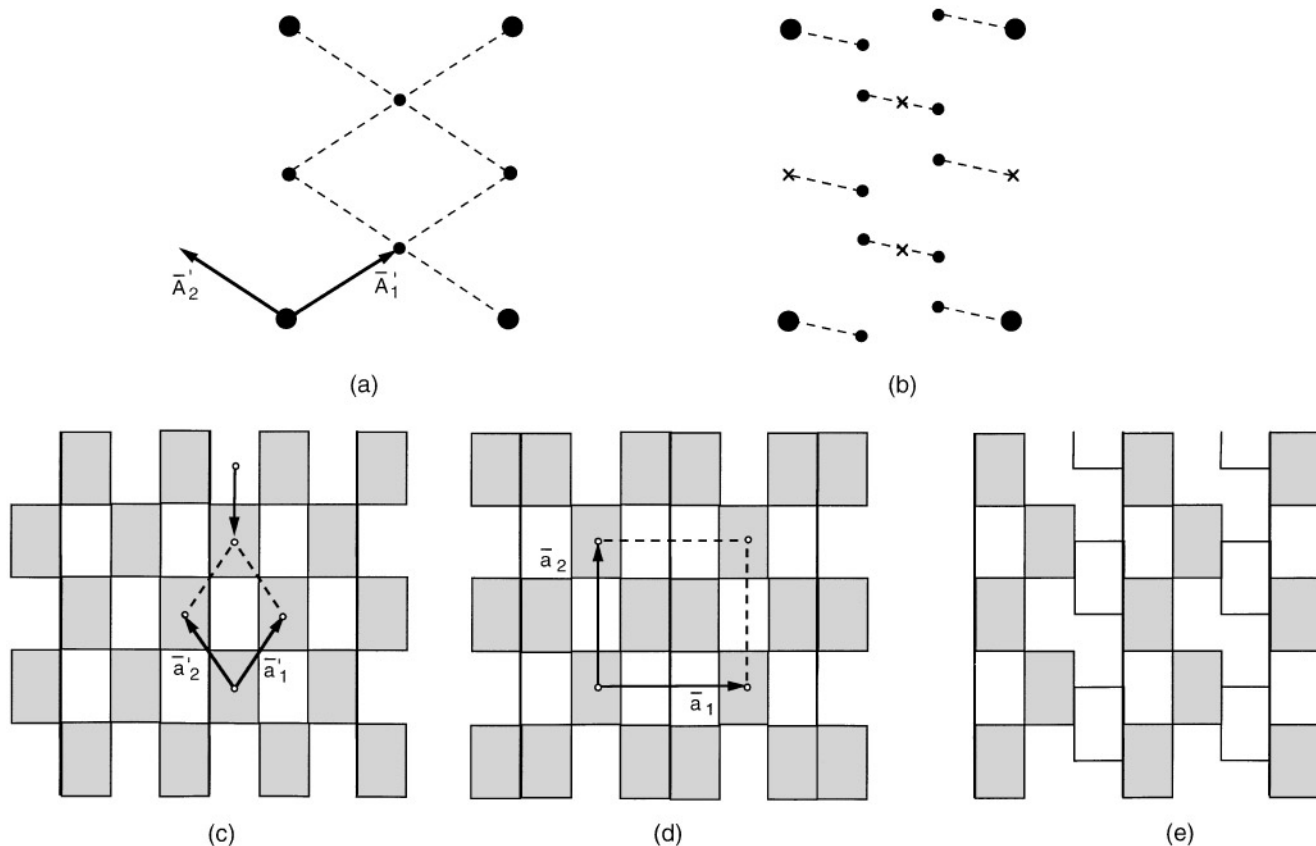

FIG. 14. Hypothetical structure of the 4M phase. (a) Diffraction pattern of the assumed basic structure. (b) Observed incommensurate diffraction pattern (Fig. 2d) of the 4M phase; the crosses indicate the positions of the basic spots. (c) Assumed basic structure consistent with the pattern of (a). (d) Interface modulated structure, derived from (c) by the shear indicated in (c). This structure, however, is not consistent with our basic assumption. (e) Structure that is consistent with these assumptions; its projection is identical to that of the 4H phase.

geometry is concerned. However, on close inspection it becomes clear that the pattern is slightly incommensurate and consists of linear equidistant satellite sequences associated with spot positions that differ from those observed in incommensurate 4H (Fig. 5c). The small orientation anomaly and its sense of inclination, together with the intensity distribution, allow us to locate the "center" of the satellite sequences and hence to determine the spot positions of the hypothetical "basic" structure. Moreover, the dense rows of spot positions are no longer strictly mutually perpendicular, even when taking into account the small orientation anomaly.

These features suggest that this structure, like that of 4H, can also be interpreted as an interface modulated structure in which the interfaces are slightly inclined with respect to the c axis. Moreover, the structure is presumably monoclinic.

The satellite sequences are indicated schematically in Figs. 5d and 14b; they are centered on the spot positions indicated by crosses. The latter can be attributed to a hypothetical simple structure, such as Fig. 14c, which would produce the diffraction pattern shown schematically in Fig. 14a. Introducing periodic parallel interfaces perpendicular to the satellite sequences, i.e., parallel to c and with a spacing of three elementary building units (indicated in Fig. 14d) and with a displacement vector $1/2(a_1 + a_2)$, leads to fractional shifts for the spot sequences given by $\mathbf{g} \cdot \mathbf{R} = 1/2 (h + k)$, in accordance with the observed diffraction pattern of Fig. 5d. The periodic interfaces and the displacement vector suggest the projected structure shown in Fig. 14d. It should be noted that this model is *not* in accordance with the structural principles postulated above. In one of the two layers the trigonal prisms project as nearest neighbors, which violates one of the empirical rules valid for this type of structure. Within the framework of these rules the proposed basic structure is nevertheless the most plausible one. The fractional shift method subsequently allows us to suggest on purely geometric grounds (from the displacement vector) the relative positions of blocks of the basic structure, as well as their limiting planes. Rearrangement, for instance along the interfaces, respecting the lattice geometry, i.e., the relationship between the blocks of basic structure, is allowed. In the present case a shift of $1/4(a_1 + a_2)$ of one of the columns (Fig. 14e) eliminates the "violation," but it produces the 4H structure. This leads us to the conclusion that the geometry of the 4M structure in this projection is the same as that of the 4H structure. However, comparing the $[01\bar{1}0]$ zone patterns of the 4H and the 4M structures (Figs. 5a, 5b) confirms that they are different structures. We have as yet not found a plausible model for the 4M structure.

The sense of inclination of the satellite sequences has apparently become opposite on forming the incommensurate 4M structure from the incommensurate 4H structure.

Since the c parameters are the same, the two structures are probably formed from the same columns, stacked in a different manner however.

7. HIGH RESOLUTION TEM

The 3R Phase

High-resolution images were obtained from the same area and along the same $[1\bar{2}10]$ zone that was used to determine the projected structures.

Individual columns of nickel atom columns could be resolved as bright dots of different brightnesses; oxygen atom columns were not revealed. The bright dots form a rectangular array with a mesh size that is the reciprocal of the rectangle of prominent reflections. Figure 15 shows the image of a band of the simplest of the observed phases, i.e., the $Ni_2Sr_3O_6$ (3R) structure represented in Fig. 13. From the rectangular configuration of the brightest dots and from its scale one can conclude that the bright dots image nickel columns. However, since in this structure the geometry of nickel columns in trigonal prismatic interstices is the same as that for nickel in the octahedral interstices, it is not possible to decide on geometric grounds alone whether one or the other type of nickel column causes the bright dots. Anyway, making this distinction is not very meaningful, since along the same band of $Sr_3Ni_2O_6$ structure a contrast inversion takes place at a thickness contour. In this transition region between both types of contrast, the bright
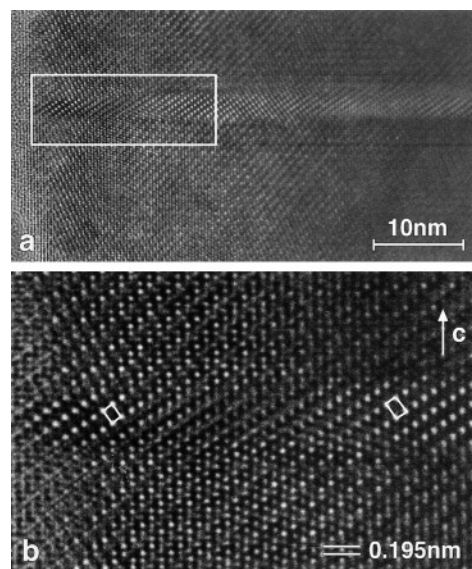

FIG. 15. Predominantly 4H, beam-heated specimen. A much simpler 3R structure is formed in a band limited by (00.1) planes. (a) Low-magnification, high-resolution image. (b) Enlarged image: the columns of nickel atoms are imaged as bright dots. The imaging code changes with thickness; in one part, the octahedral columns are imaged; in the other part, the trigonal prismatic columns are imaged.
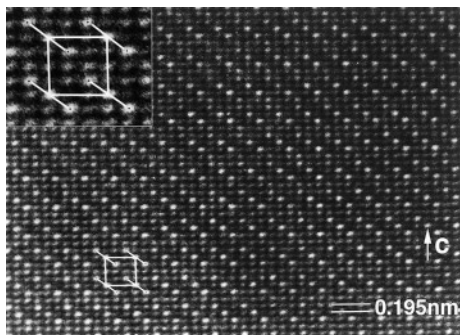
FIG. 16. High-resolution image of the commensurate 4H phase. One projected unit cell is outlined. The brightest dots image nickel columns in trigonal prismatic interstices. The outlined unit mesh can be compared with the unit mesh in Fig. 8b and also with the simulated image of Fig. 17.

FIG. 17. Calculated HREM images for the 4H structure for different defocus values and different thicknesses of the sample.

dots form a centered rectangle; both types of columns are now imaged. The matrix surrounding this band consists of the 9R structure as we shall see.

The 4H Structure

Figure 16 refers to the 4H structure. Again, the prominently bright dot pattern is a subpattern of a finer rectangular lattice of bright dots with different intensities. The mesh of this fine-scale dot pattern is the reciprocal of the rectangle of prominent reflections. From the size and scale of the pattern of prominently bright dots one can deduce unambiguously that, under the conditions used there, these dots image columns consisting of nickel in trigonal prismatic interstices and of strontium. This image thus confirms the structure model of Figs. 7 and 2.

8. IMAGE SIMULATIONS AND IMAGING CODE

To validate a suitable imaging code, image simulations were performed for the commensurate 4H structure, according to the structural data from (15). A matrix of images, computed by means of the Mac Tempas program is represented in Fig. 17, considering various defocus values. Focusing attention on the linear triplet of bright dots in the image taken at $\Delta f = -700$ Å and at a thickness of 50 Å, one finds that such triplets form a rectangular lattice. Comparing this configuration of bright dots with the structural model of Fig. 7, it becomes evident that under these imaging conditions the bright dots can be attributed to columns of nickel in the centers of trigonal prismatic interstices, which also contain strontium. A consistent application of this imaging code to images taken under similar conditions leads to confirmation of the proposed structure.

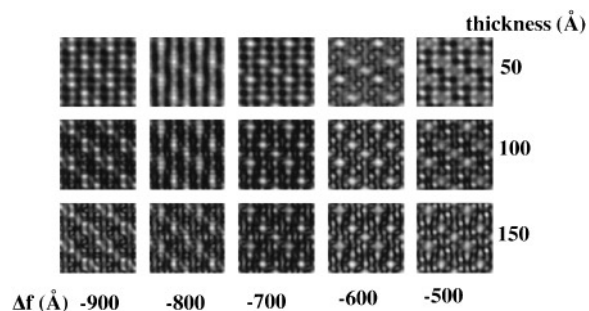However, the image of the 3R structure in Fig. 15 demonstrates that a change in the thickness may cause a change in the imaging code. Whereas at small foil thickness the bright dots represent nickel columns in octahedral interstices and strontium, at a larger foil thickness they represent nickel atoms in trigonal prismatic interstices. According to the structure model (Fig. 13) both configurations of columns have the same geometry and are related only by a translation. A distinction on pure geometric grounds is thus not possible. Within the thickness contour all columns are imaged.

The bright dots in Fig. 16 are arranged on a quasi-square lattice; however, their brightness varies periodically according to a two-dimensional superlattice with the same mesh as that of the projected structure. The columns centered on trigonal prismatic sites form in general a different subset of a similar quasi-square lattice, shifted along the c direction over one-half of a layer thickness, with respect to that of the octahedral interstices.

When both types of columns are imaged one thus finds zig-zag arrangements of dots along the lines perpendicular to the c axis. The geometry of the prominently bright dot configuration thus allows us, in many cases, to decide which type of column is being imaged.
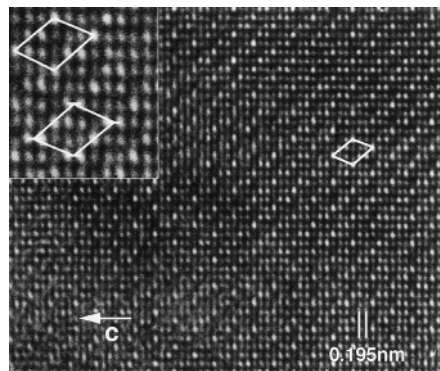

FIG. 18. High-resolution image of the 9R phase. The projected unit mesh is indicated. This image is to be compared with Fig. 5. Note that all bright dots are on a rectangular lattice with the elementary unit mesh. The brightest dots image columns of Ni in octahedral interstices.
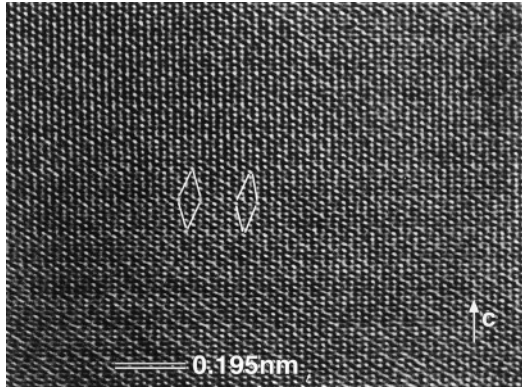
FIG. 19. High-resolution image of the 18R phase. The projected unit mesh is indicated. This image can be compared with the schematic of Fig. 9b.

The difference in imaging behavior with specimen thickness of nickel ions in a different oxygen coordination is presumably a consequence of the difference in charge state of the nickel ions (4^+ and 2^+), since the linear density of nickel ions along the columns is the same in both cases.

The image in Fig. 18 refers to the 9R structure. Also in this case the bright dots form a quasi-square array, the brightness of the dots being periodically modulated in two dimensions with the projected unit mesh deduced from the diffraction pattern. The brightest dots among them can consistently be assimilated with the Sr-configuration inbetween the Ni columns. The relative brightness of the dots is indicated by open dots of variable size, with respect to the model in Fig. 11. The prominently bright dots in Fig. 18, marking the threefold period along the layer planes, are seen to shift sideways in the way suggested by the model of Fig. 11.

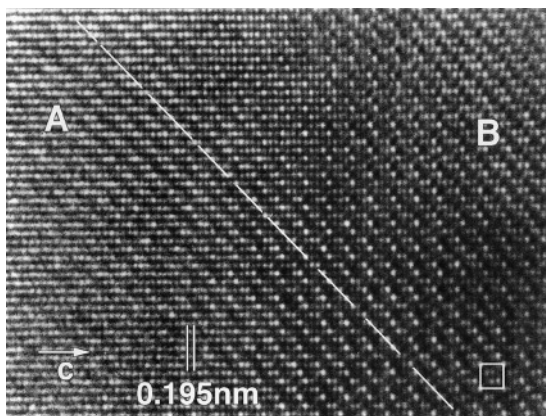The image in Fig. 19 refers to a sample exhibiting the 18R diffraction pattern. The bright dots do not form a rectangular pattern; whereas the vertical rows are straight, the horizontal rows have a zig-zag shape. In this case all nickel columns seem to be imaged and no prominent unit mesh imposes itself.

Figure 20 was produced by a region exhibiting an incommensurate diffraction pattern. The bright dot pattern allows to conclude that in part A the 4H structure is present; the imaging code being the same as in Fig. 16. The loci of pronounced bright dots form broad fringes which gradually bend in region B, which is responsible for the incommensurate pattern.

9. DIFFUSE SCATTERING

A number of $[11\bar{2}0]$ zone diffraction patterns, especially after heat treatment in the microscope, exhibit diffuse lines along two mutually perpendicular directions. One set is parallel to the c^* axis and the other one is perpendicular to it. Both line systems pass through the main diffraction spots (Fig. 21).

The diffuse lines parallel to the c^* direction show reinforcements at positions that correspond to multiples of the interlayer spacing. This set of diffuse lines must be attributed to one-dimensional disorder in the stacking of (00.1) layers. Possible faults are triplets of layers in either the *ABABCBC* or *ABABCACA* configuration within the normal *ABAB* ... stacking. Since such diffuse lines grow more intense during heating a sample (Fig. 6d) it is very probable that such faults are also generated in the heating process. This would imply a shear process along (00.1) planes. However, disorder in the arrangement of the planar interfaces of the type assumed to occur in the 9R and 18R structures may also be responsible.
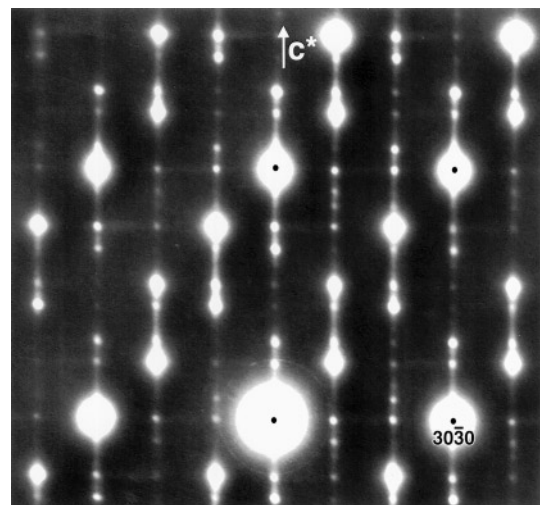

FIG. 20. High-resolution image of the incommensurate 4H phase (upper left) in contact with a commensurate part (lower right). Note the bending of lattice rows due to ledging.

FIG. 21. Incommensurate 4H diffraction pattern along the $[1\bar{2}10]$ zone, showing pronounced diffuse intensity along c^* as well as perpendicular to c^*.

The faint diffuse lines perpendicular to c^* must presumably be attributed to intersection with diffuse planes perpendicular to c^* in reciprocal space. Such diffuse planes can be caused by longitudinal positional disorder of the columns of oxygen polyhedra. This type of disorder is coupled to the one-dimensional disorder of layers; the occurrence of one type implies the occurrence of the other type.

The absence of diffuse scattering in the [00.1] zone diffraction pattern is consistent with this interpretation.

10. DISCUSSION AND CONCLUSIONS

An electron microscopy and electron diffraction study has revealed that the compound with composition around $Sr_4Ni_3O_9$ may occur as several closely related microphases, the structures of which are based on the presence of one-dimensional strings consisting in part of face sharing octahedra and in part of trigonal prisms sharing faces with the octahedra. Alternatively, the structures can also be described in terms of the stacking of close-packed layers of the type Sr_3O_9 with omission.

In the chains parallel to the layer normals, the trigonal prisms always seem to occur isolated, whereas the octahedra occur either singly or in face-sharing pairs. In other related compounds longer strings of face-sharing octahedra may occur (1). Prisms as well as octahedra can be occupied by nickel.

The HREM observations were interpreted using an imaging code obtained by comparison of the computer-simulated image of the 4H phase, based on the structure known from X-ray diffraction, with the observed images. The structure of the 4H phase can be derived from that of a simpler structure modulated by the periodic insertions of planar translation interfaces with a displacement vector $1/4c$.

It is shown that the diffraction pattern of the "modulated" structure has the correct geometry and the correct intensity distribution. In this manner it was possible to attribute the occurrence of slightly incommensurate diffraction patterns to the systematic "ledging", i.e., to sideways shifting of the translation interfaces in the manner first observed in long-period antiphase boundary modulated structures of ordered alloys (18, 19). A change in the average orientation of the interfaces results in a change in orientation of the linear arrays of modulation satellites.

After *in situ* heating, the samples are inhomogeneous, even at nanoscale. The same area may exhibit different phases in adjacent regions from the HREM image.

REFERENCES

1. J. Darriet and M. A. Subramanian, *J. Mater. Chem.* **5,** 543 (1995).
2. Y. Takeda, F. Kanamuru, M. Shimada, and M. Koizumi, *Acta Crystallogr.* **32,** 2464 (1976).
3. P. C. Donohue, L. Katz, and R. Ward, *Inorg. Chem.* **4,** 306 (1965).
4. R. D. Burbank and H. T. Evans, *Acta Crystallogr.* **1,** 330 (1948).
5. P. S. Haradem, B. L. Chamberland, and L. Katz, *J. Solid State Chem.* **34,** 59 (1980).
6. J. J. Randall and L. Katz, *Acta Crystallogr.* **12,** 519 (1959).
7. S. J. Schneider and C. L. McDaniel, *J. Am. Ceram. Soc.* **52,** 518 (1969).
8. C. L. McDaniel and S. J. Schneider, *J. Res. Natl. Bur. Stand. Sect. A* **75,** 185 (1971).
9. J. A. Campa, E. Gutierrez-Puebla, M. A. Monge, I. Rasines, and C. Ruiz-Valero, *J. Solid State Chem.* **108,** 230 (1994).
10. J. Campa, E. Gutierrez-Puebla, A. Monge, I. Rasines, and C. Ruiz-Valero, *J. Solid State Chem.* **126,** 27 (1996).
11. C. Dussarrat, J. Fompeyrine, and J. Darriet, *Eur. J. Solid State Inorg. Chem.* **32,** 3 (1995).
12. M. Strunk and H. Müller-Buschbaum, *Z. Anorg. Allg. Chem.* **620,** 1565 (1994).
13. M. Strunk and H. Müller-Buschbaum, *J. Alloys Comp.* **209,** 189 (1994).
14. J. Lee and G. F. Holland, *J. Solid State Chem.* **93,** 267 (1991).
15. F. Abraham, S. Minaud, and C. Renard, *J. Mater. Chem.* **4,** 1763 (1994).
16. G. Van Tendeloo, S. Amelinckx, B. Darriet, R. Bontchev, J. Darriet, and F. Weill, *J. Solid State Chem.* **108,** 314 (1994).
17. S. Amelinckx, J. Van Landuyt, and G. Van Tendeloo, *in* "Modulated Structure Materials" (T. Tsakalakos, Ed.), p. 183. Martinus Nijhoff, Dordrecht, 1984.
18. G. Van Tendeloo and S. Amelinckx, P*hys. Status Solidi A* **43,** 553 (1977).
19. D. Broddin, G. Van Tendeloo, and S. Amelinckx, *J. Phys. Cond. Matter* **2,** 3459 (1990).